NOTES AND CORRESPONDENCE

The Role of Meltwater Advection in the Formulation of Conservative Boundary Conditions at an Ice–Ocean Interface

ADRIAN JENKINS

British Antarctic Survey, Natural Environment Research Council, Cambridge, United Kingdom

HARTMUT H. HELLMER

Alfred Wegener Institute for Polar and Marine Research, Bremerhaven, Germany

DAVID M. HOLLAND

Courant Institute of Mathematical Sciences, New York University, New York, New York

23 July 1999 and 10 July 2000

ABSTRACT

Upper boundary conditions for numerical models of the ocean are conventionally formulated under the premise that the boundary is a material surface. In the presence of an ice cover, such an assumption can lead to nonconservative equations for temperature, salinity, and other tracers. The problem arises because conditions at the ice–ocean interface differ from those in the water beneath. Advection of water with interfacial properties into the interior of the ocean therefore constitutes a tracer flux, neglect of which induces a drift in concentration that is most rapid for those tracers having the lowest diffusivities. If tracers are to be correctly conserved, either the kinematic boundary condition must explicitly allow advection across the interface, or the flux boundary condition must parameterize the effects of both vertical advection and diffusion in the boundary layer. In practice, the latter alternative is often implemented, although this is rarely done for all tracers.

1. Introduction

Exchanges of heat and freshwater at the surface of the ocean represent the major forcing behind the creation of new water masses. In the polar oceans, the source regions for most of the deep and bottom waters, the processes of exchange are strongly influenced by the presence of ice. If ocean models are to simulate the characteristics and distribution of abyssal waters correctly, they must include an adequate representation of the coupling between ice and ocean. Because melting and freezing entail a transfer of water between the two media, this coupling formally manifests itself in the boundary conditions placed on both the vertical velocity and on the tracer concentrations. However, it is an almost universal practice in numerical modeling of the ocean to regard the sea surface as a permeable, but material, interface—properties may diffuse across it, but no water may be exchanged between the ocean and the overlying medium, be it atmosphere or ice. Huang (1993) criticized such practice, on the grounds that it suppresses the Goldsburgh–Stommel circulation and recommended setting the vertical velocity relative to the upper boundary equal to the precipitation, evaporation, melt, or freeze rate. Here we examine what the assumed nature of the ocean surface implies for the balance equations for tracers under conditions of melting and freezing.

The ice–ocean boundary layer is a region that is distinguished by relatively high gradients in tracer concentrations combined with large changes in the effective diffusivity. It is often the case that the equations used to describe the transport of tracers in the bulk of the oceanic water column are not applicable in the boundary region. This problem can be circumvented by incorporating a simple parameterization of the boundary layer processes into the boundary conditions. Such a formulation invariably entails the diagnosis of conditions at the ice–ocean interface that are distinct from those pertaining at the uppermost model grid point within the

Corresponding author address: Dr. Adrian Jenkins, British Antarctic Survey, Natural Environment Research Council, High Cross, Madingley Rd., Cambridge CB3 0ET, United Kingdom.
E-mail: a.jenkins@bas.ac.uk

sub-ice water column. In the presence of such differences, the advection of meltwater into the bulk of the ocean plays an important role in the balance equations for tracers, but the advective flux is formally absent if the ice–ocean interface is treated as a material surface.

We use a simple, one-dimensional model of the ocean beneath sea ice to demonstrate the role played by meltwater advection in the conservation of tracers. To this model we apply two sets of boundary conditions that differ only in the assumption made about the nature of the ice–ocean interface: material or not. We also discuss the two-dimensional model of thermohaline circulation beneath an ice shelf presented by Hellmer and Olbers (1989) and Hellmer et al. (1998). This model has a material interface at the ice–ocean boundary, but changing the kinematic boundary condition would entail a considerable increase in complexity. Instead, we include the effect of meltwater advection through a modified flux boundary condition and show that this simple fix improves the model performance. Finally, we discuss how the boundary formulations discussed here compare with those used elsewhere.

2. Fundamental equations

Our discussion will focus on the evolution of scalar properties in the upper ocean, and we will use the following generic equation to model this evolution:

$$\frac{\partial X}{\partial t} + \boldsymbol{\nabla} \cdot (\mathbf{u}X) + \frac{\partial}{\partial z}(wX) = -\boldsymbol{\nabla} \cdot \langle \mathbf{u}'X' \rangle - \frac{\partial}{\partial z}\langle w'X' \rangle, \tag{1}$$

where X could be temperature T, salinity S, or any other conservative tracer; boldface variables represent horizontal vectors; primed variables represent turbulent fluctuations; and angle brackets indicate ensemble averaging. In the presence of an ice cover, this equation is forced by the upper boundary conditions placed on the terms describing the vertical advection and diffusion of tracers.

The advective flux at the ice–ocean interface is simply

$$(wX)|_b = w_b X_b, \tag{2}$$

where the subscript b indicates conditions at the ice–water contact. For a nonmaterial surface, the vertical velocity at the boundary is derived from a combination of the motion of the boundary and the advection of fluid across the boundary:

$$w_b = \frac{\partial z_b}{\partial t} + \mathbf{u}_b \cdot \boldsymbol{\nabla} z_b - m, \tag{3}$$

where m indicates the melt rate (negative for freezing) expressed as a thickness of seawater per unit time. For the more commonly encountered material interface, the particles lying on the boundary at one time must lie there at all subsequent times, so their motion must be equal to that of the boundary itself:

$$w_b = \frac{\partial z_b}{\partial t} + \mathbf{u}_b \cdot \boldsymbol{\nabla} z_b. \tag{4}$$

Under this assumption the melt/freeze rate does not impact the continuity equation, a simplification that explains why (4) is generally favored over (3). The price to be paid for this simplification is a slight inconsistency between the continuity and tracer equations because the impact of melting and freezing must be retained in the latter.

We express the diffusive flux at the ice–ocean interface as the product of a turbulent transfer coefficient and the difference in the tracer concentration across the surface boundary layer:

$$\langle w'X' \rangle|_b = \gamma_X (X - X_b), \tag{5}$$

where the transfer coefficient γ_X has the dimensions of velocity (i.e., diffusivity over length). Since the surface boundary layer itself is part of the ocean domain, the precise meaning of the transfer coefficient depends on the form of discretization applied to (1). In a layer model, X in (5) will be a depth-averaged value across the upper layer, part of which will be the boundary layer, and the value of γ_X should reflect this. In a level model, X will be the value at the first level below the boundary, and the value of γ_X should reflect whether this point is within or outside of the boundary layer. At vertical resolutions commonly used in ocean models, these distinctions are unimportant because most of the change in tracer concentration occurs across a very thin viscous sublayer (McPhee 1990). The result is that conditions at the upper level, or within the upper layer, of a model are practically equivalent to the far-field conditions outside the boundary layer.

The application of Eqs. (2) and (5) requires knowledge of the tracer concentration at the ice–ocean interface. We derive this from a consideration of the budget within an infinitesimal control volume that straddles the interface (Mellor et al. 1986). We demand an exact balance between the vertical diffusive fluxes and the sources or sinks of the tracer represented by the consumption or production of meltwater within the control volume:

$$\rho_i k_i \left.\frac{\partial X_i}{\partial z}\right|_b - \rho \gamma_X (X_b - X) = \rho m (X_b - X_i). \tag{6}$$

Here the subscript i indicates ice properties, ρ are densities, and k is a diffusivity. For most tracers, including salinity, stable isotopes and incorporated gases, the diffusivity in ice is negligible, so the first term on the left-hand side of (6) vanishes. This is not so in the case of temperature, for which Eq. (6) becomes

$$\rho_i c_i k_i \left.\frac{\partial T_i}{\partial z}\right|_b - \rho c \gamma_T (T_b - T) = \rho m L_i, \tag{7}$$

where c are specific heat capacities and L a latent heat of fusion.

Complete specification of the boundary problem re-

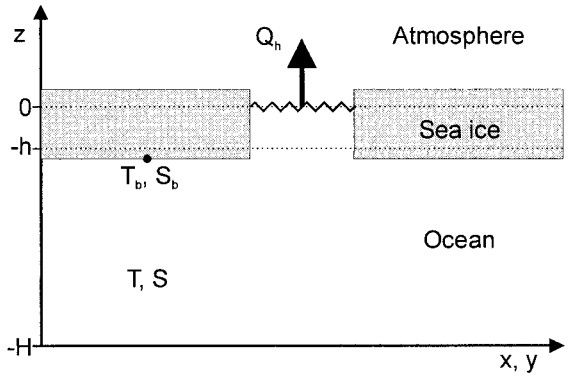

FIG. 1. Schematic of a one-layer ocean beneath sea ice. The ocean layer is characterized by a single temperature and salinity (T, S) and is forced by an atmospheric heat flux (Q_h) that passes through leads. The temperature and salinity at the ice–ocean interface (T_b, S_b) differ from those in the interior, and the differences drive melting and freezing. The sea ice is regarded as a continuum, so the ice–ocean boundary conditions and the atmospheric heat flux are formally applied at the level of the mean ice draft ($z = -h$). The seabed lies at $z = -H$.

quires an expression for the melt/freeze rate. This is determined by the rate at which heat and salt are supplied to, or extracted from, the control volume, and can be calculated from the combination of (7), with an appropriate specification or parameterization of heat conduction through the ice, and the salinity version of (6). A third constraint is that the seawater within the control volume must be at the freezing point, which we define using a linear equation:

$$T_b = \lambda_1 S_b + \lambda_2 + \lambda_3 P_b, \tag{8}$$

where P_b is the pressure at the interface and λ_{1-3} are constants: -0.0573°C/psu, 0.0832°C, and -7.53×10^{-8} °C/Pa, respectively. This relationship is based on that of Millero (1978), with the salinity dependence linearized. Equations (6)–(8) can be solved simultaneously for m, S_b, and T_b, a procedure that is simplified by the use of a linear equation in (8). With the melt rate known the boundary concentration of any other tracer can be calculated from (6) if the concentration in the ice is known.

Boundary conditions of the form given in (5)–(8) were introduced by Josberger (1983) and McPhee (1983). Mellor et al. (1986) recognized the importance of molecular diffusion within the viscous sublayer in determining the melt/freeze rate, and McPhee et al. (1987) and Steele et al. (1989) investigated expressions for the turbulent transfer coefficients that included explicit parameterizations of this process. The magnitudes of the transfer coefficients used in this study are derived from the results of this pioneering work.

3. A simple model of the ocean beneath sea ice

We begin by considering the evolution of a one-layer ocean model (Fig. 1) subject to a symmetric cycle of heating and cooling. We assume horizontal homogeneity and treat the lower boundary as a fixed, insulating surface, thus isolating the upper boundary condition as the only forcing on the model. Under these assumptions integration of Eq. (1) over the depth of the water column leads to

$$\int_{-H}^{-h} \frac{\partial X}{\partial t}\, dz + w_b X_b = -\langle w'X' \rangle|_b. \tag{9}$$

The integral expression can be evaluated as

$$\int_{-H}^{-h} \frac{\partial X}{\partial t}\, dz = \frac{\partial}{\partial t}[(H - h)\overline{X}] + X_b \frac{\partial h}{\partial t}, \tag{10}$$

where the overbar indicates a depth-averaged quantity, and we have made use of the Leibnitz theorem for the differntiation of an integral.

If there were complete ice coverage, the turbulent fluxes at the upper boundary would take the form given in (5) but, if direct ocean–atmosphere exchange can take place through leads, the flux boundary condition at the ice–ocean interface ($z = -h$) becomes

$$\rho\langle w'X' \rangle|_b = A\rho\gamma_X(\overline{X} - X_b) + (1 - A)Q_X, \tag{11}$$

where A is the areal fraction of the surface covered by ice and Q_X is the tracer flux passing through the leads. In the temperature equation, Q_X is replaced by Q_h/c, where Q_h is the heat flux. The two choices for the remaining advective boundary condition are discussed separately below.

We force the model with a sinusoidal variation in the atmospheric heat flux having an amplitude of 500 W m^{-2} over open water and a period of one year. For all other tracers we assume that the flux passing through the leads is zero. The water column thickness ($H - h$) is initially 50 m and the ocean has an initial salinity of 34.5 psu and an initial temperature at the appropriate salinity-dependent freezing point. The initial ice thickness is arbitrary, as we are only concerned with how the melting and freezing cycle influences the bulk ocean properties. The areal coverage of ice is assumed constant at 90% and the model is run for 10 years. We use a turbulent heat transfer coefficient, γ_T, of 5×10^{-5} m s^{-1} and a turbulent salt transfer coefficient, γ_S, of $0.04\gamma_T$. These values are appropriate for a moderate friction velocity of 5×10^{-3} m s^{-1} (McPhee et al. 1987; Holland and Jenkins 1999).

For the purposes of diagnosing the melt/freeze rate and the temperature and salinity at the ice–ocean boundary, we assume that no salt is incorporated into the ice on freezing. We also assume the ice to be sufficiently thick that the heat conducted through it is negligible, which allows us to set the first term on the left-hand side of (7) to zero. The pressure-dependent term in (8) can also be neglected. Note that these assumptions, along with the simple formulations we have used for the heat and salt transfer coefficients, do not affect the form of the equations presented below. They influence only the magnitude of the forcing.

a. With meltwater advection

We first regard the ice–ocean boundary as a nonmaterial interface and apply a kinematic boundary condition of the form given in (3):

$$w_b = -\frac{\partial h}{\partial t} - Am. \tag{12}$$

Applying this and the flux boundary condition given in (11) to (9), the conservation equation for a generic tracer becomes

$$\frac{\partial}{\partial t}[(H - h)\overline{X}] - AmX_b = A\gamma_X(X_b - \overline{X}) - (1 - A)\frac{Q_X}{\rho}. \tag{13}$$

The vertical velocity must vanish at the seabed, so our assumption of zero gradient in the horizontal velocity field implies that the w_b must also be zero, and (12) can be rewritten:

$$\frac{\partial}{\partial t}(H - h) = Am \tag{14}$$

because H is fixed for all time. Using (14) to expand the derivative on the left-hand side of (13), the model equations for salinity and temperature, respectively, become

$$\frac{\partial \overline{S}}{\partial t} = \frac{A(\gamma_S + m)}{(H - h)}(S_b - \overline{S}) \tag{15a}$$

$$\frac{\partial \overline{T}}{\partial t} = \frac{A(\gamma_T + m)}{(H - h)}(T_b - \overline{T}) - \frac{(1 - A)Q_h}{\rho c(H - h)}. \tag{15b}$$

Results obtained with this version of the model are shown in Fig. 2. The annual cycle in ice thickness shows a peak-to-peak range of about 1.5 m, giving rise to ocean salinities that cycle over a range of about 1 psu. Ocean temperatures deviate by up to 0.35°C from the freezing point. The maxima and minima in ice thickness occur about 2.5 weeks after the change in sign of the atmospheric heat flux in spring and autumn (Fig. 2a). The lag is approximately equal to the reaction time, τ, of the oceanic layer:

$$\tau = \frac{(H - h)}{\gamma_{T\text{eff}}}, \tag{16}$$

where $\gamma_{T\text{eff}}$ is the effective heat transfer coefficient, defined by Holland and Jenkins (1999) as

$$\gamma_{T\text{eff}} = \gamma_T\left(1 - \frac{\lambda_1(S_b - S_i)c\gamma_T}{L_i\gamma_S}\right)^{-1}. \tag{17}$$

Continual relaxation towards the freezing point means that the water temperature is a function of the rate at which heat is lost to, or gained from, the atmosphere, subject to the lag mentioned above, so the temperature extremes occur shortly after midsummer and midwinter (Fig. 2b). The salinity is a function of the cumulative heat loss or gain throughout a growth or melt season, so the extremes occur when freezing switches to melting, and vice versa. Together these signatures give an annual cycle that traces an ellipse (counterclockwise) in temperature/salinity space. This cycle does not exactly repeat itself. There is a drift of about 0.0025 psu yr^{-1} toward lower salinities, consistent with a reduction in ice thickness of approximately 4 mm yr^{-1}. This drift arises because the ice cover is thicker on average during the spring to autumn period of heating than during the autumn to spring period of cooling (Fig. 2a). In this model formulation the water lost by the ice during melting is gained by the ocean, and vice versa during freezing. The water column is therefore thinner and has a smaller heat capacity, on average, during periods of heating than during periods of cooling, and this allows slightly more melting to occur than freezing.

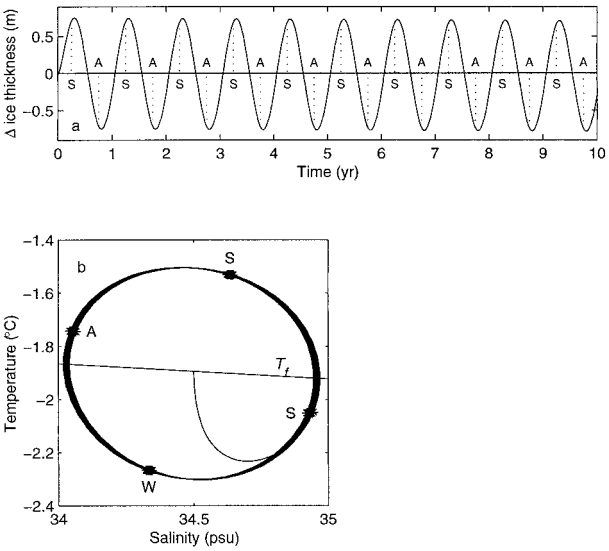

FIG. 2. Results of a ten-year integration of (15): (a) change in ice thickness, (b) temperature, and salinity of the ocean. In (a) the dotted lines indicate the time at which the atmospheric heat flux changes sign in spring (S) and autumn (A). In (b) the stars labeled S (spring), S (summer), A (autumn), W (winter) indicate the times of maximum and zero atmospheric forcing, while the straight line labelled T_f indicates the freezing point at atmospheric pressure.

Despite the simplicity of the model we find some support for such a cycle of ocean properties in observations made during the Arctic Ice Dynamics Joint Experiment. Figure 3 shows mixed layer temperatures and salinities recorded daily between late May 1975 and mid-April 1976 at the Snowbird station (Maykut and McPhee 1995). Many factors not considered in our one-dimensional model, such as drift of the station, horizontal advection of water masses, mixing across the pycnocline, variations in ice concentration, and a variable input of turbulent kinetic energy to the ocean with the passage of weather systems, will all have influenced the observations. Given these complicating factors, the basic shape and phasing of the observed annual cycle

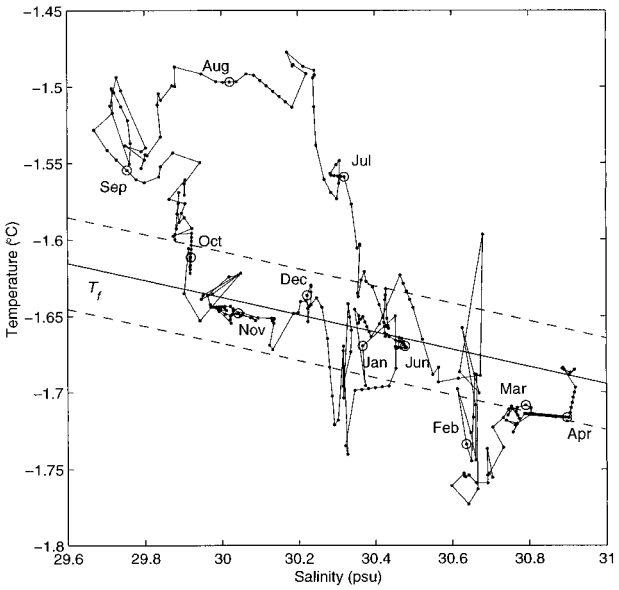

FIG. 3. A 331-day record of temperature and salinity at the Snowbird ice camp. Each dot represents an average value for the upper 25 m of the water column. Data from the first day of each month are circled and labeled. The straight line labeled T_f indicates the freezing point at atmospheric pressure, and the two dashed lines indicate the likely uncertainty in the observed deviation from the freezing point (Maykut and McPhee 1995).

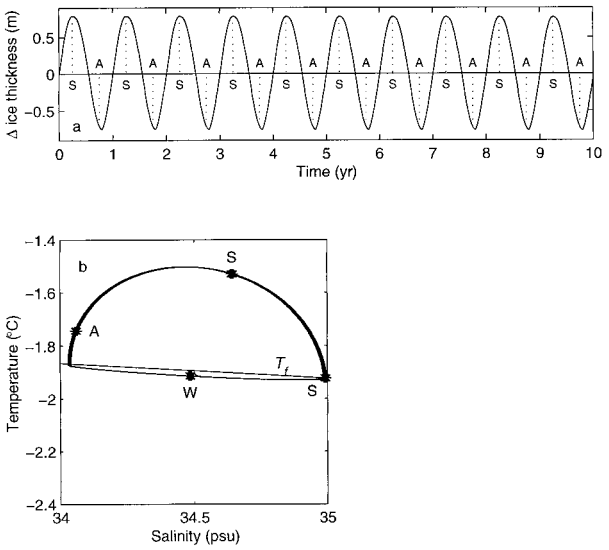

FIG. 4. Same as Fig. 2 but with heat and salt transfer coefficients increased by a factor of 20 when the ocean temperature falls below the freezing point.

in mixed layer properties compare favorably with the model results.

The main qualitative difference between the observations and model results is the lack of any sustained period of supercooling, at levels above the detection threshold of the instrumentation used, in the observational record. A lack of supercooling suggests that the ocean response time is shorter during periods of ice growth than during periods of melting. The reason may be frazil ice production in the water column or fundamentally different behavior within the boundary layer when salt, rather than freshwater, is produced at the phase change interface. Whatever the physical mechanism, we can simulate the effect in the model by increasing the magnitude of the heat and salt transfer coefficients during periods of supercooling. The results are shown in Fig. 4. With the wintertime response of the ocean 20 times faster than before, supercooling is restricted to no more than about 0.02°C, and the peak in supercooling and the transition from melting to freezing are practically coincident with the maximum and the change in sign, respectively, of the atmospheric forcing. Because there is little phase lag between the cycles of atmospheric heat flux and ice growth during half of the year, the drifts in ice thickness and ocean salinity are reduced by a factor of 2.

b. Without meltwater advection

We next treat the ice–ocean boundary as a material surface and apply a kinematic boundary condition analogous to (4):

$$w_b = -\frac{\partial h}{\partial t}. \tag{18}$$

Applying this and the flux boundary condition given in (11) to (9) gives

$$\frac{\partial}{\partial t}[(H - h)\overline{X}] = A\gamma_X(X_b - \overline{X}) - (1 - A)\frac{Q_X}{\rho} \tag{19}$$

for a genetic tracer. Equating w_b to zero yields

$$\frac{\partial}{\partial t}(H - h) = 0, \tag{20}$$

and the model equations for salinity and temperature become

$$\frac{\partial \overline{S}}{\partial t} = \frac{A\gamma_S}{D}(S_b - \overline{S}) \tag{21a}$$

$$\frac{\partial \overline{T}}{\partial t} = \frac{A\gamma_T}{D}(T_b - \overline{T}) - \frac{(1 - A)Q_h}{\rho c D}, \tag{21b}$$

where $D = H - h$ is the, now temporally constant, water column thickness.

The main differences between (15) and (21) arise because the water advected into or out of the ocean in (15), which is absent in (19), has properties equal to those at the boundary. Advection therefore constitutes a tracer flux that is additional to the diffusive fluxes given by (5). Using (21) we obtain a similar evolution of the ice cover to that obtained with (15), but we find a rapid drift of about 0.1 psu yr^{-1} toward higher salinity (Fig. 5). The increase in salinity is what we would anticipate for a net ice growth of 15 cm yr^{-1}, and is clearly in error. It is a result of the missing advective fluxes, which are expressed as the products of the melt rate and

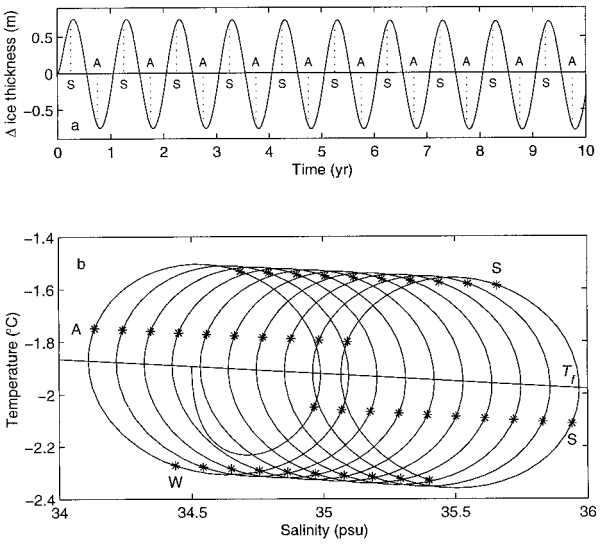

FIG. 5. Results of a ten-year integration of (21): (a) change in ice thickness, (b) temperature, and salinity of the ocean. In (a), the dotted lines indicate the time at which the atmospheric heat flux changes sign in spring (S) and autumn (A). In (b), the stars labeled S (spring), S (summer), A (autumn), W (winter) indicate the times of maximum and zero atmospheric forcing, while the straight line labeled T_f indicates the freezing point at atmospheric pressure.

the difference in tracer concentration between the mixed layer and the ice–ocean interface [Eq. (15)]. The concentration differences are generated by the rejection or uptake of tracers during freezing or melting, so they change sign synchronously with the melt rate (Fig. 6). Hence, the advective fluxes are always of the same sign, and, although they are generally small, their neglect leads to an error that accumulates throughout the annual cycle. With the reaction time of the ocean shortened by

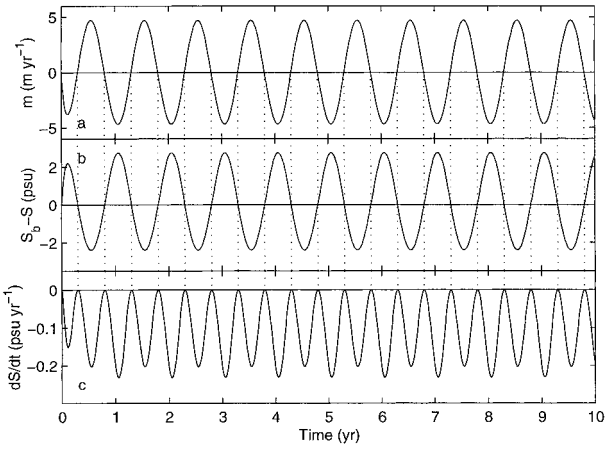

FIG. 6. Illustration of the net dilution induced by advection of meltwater into an ocean layer having a nonmaterial upper boundary: (a) melt rate, (b) salinity difference across the ice–ocean boundary layer, and (c) salinity change that results from the inclusion of meltwater advection on the right-hand side of (15a), defined by $dS/dt = Am(H - h)^{-1}(S_b - \overline{S})$. Dotted lines indicate the times at which the melt rate changes sign.

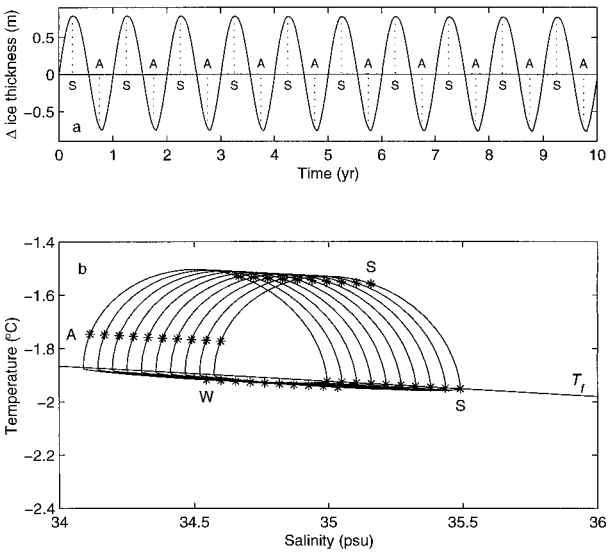

FIG. 7. Same as Fig. 5 but with heat and salt transfer coefficients increased by a factor of 20 when the ocean temperature falls below the freezing point.

a factor of 20 during freezing, the difference in salinity across the boundary layer, and hence the salt flux error, is reduced in winter. The annual drift in salinity is therefore approximately halved (Fig. 7).

Although the net salinity drift is a function of our model setup, in particular the choice of water column thickness, the magnitude of the flux errors are determined only by the nature of the ice–ocean boundary conditions. In the appendix we develop general expressions for the size of the errors and demonstrate that they are approximately proportional to the square of the deviation in water temperature from the freezing point. The errors are most significant for slowly diffusing tracers with small γ_X, the ratio of the excluded advective to included diffusive fluxes being m/γ_X. For this reason the salinity error is much more apparent in Figs. 5 and 7 than the temperature error. The solution could not drift from the freezing point line in any case, but the heat flux error alone would act to reduce the thickness of the ice cover and freshen the mixed layer.

4. A model of thermohaline circulation beneath an ice shelf

We next consider the model of thermohaline circulation beneath an ice shelf described by Hellmer and Olbers (1989). The model domain consists of a vertical plane, oriented perpendicular to the ice front and extending into the cavity beneath the ice shelf. The boundary located at the ice front is open, while the interior boundaries are fixed material surfaces, the upper one corresponding to the ice shelf base. A single equation for the vertical streamfunction replaces the momentum and continuity equations, while the generic equation for tracers, equivalent to our Eq. (1), is written

$$\frac{\partial X}{\partial t} + \frac{\partial}{\partial y}(vX) + \frac{\partial}{\partial z}(wX) = \frac{\partial}{\partial y}\left(K_H \frac{\partial X}{\partial y}\right) + \frac{\partial}{\partial z}\left(K_V \frac{\partial X}{\partial z}\right) + C, \tag{22}$$

where v and w are horizontal and vertical components of velocity, K_H and K_V are horizontal and vertical eddy diffusivities, and C indicates a convective term used to eliminate static instability. Boundary conditions on the streamfunction are specified such that there is no normal flow at the solid boundaries and only normal flow at the open boundary, where the model is forced with an observed vertical profile of temperature and salinity. Where outflow occurs, the observations are overwritten by values advected from the cavity interior. Heat and salt balances at the ice shelf base are specified as in Eqs. (6) and (7), with the first term on the left-hand side of (7) parameterized in a manner appropriate for heat conduction into a melting ice shelf (Nøst and Foldvik 1994; Holland and Jenkins 1999):

$$\rho_i c_i k_i \left.\frac{\partial T_i}{\partial z}\right|_b = \rho m c_i (T_s - T_b), \tag{23}$$

where T_s is the temperature at the surface of the ice shelf.

The model equations are solved on a rectangular grid with regular horizontal and vertical spacing. Staggering of the grid means that the vertical velocity is defined on points that lie half a grid cell above and below the points carrying the tracers. The ice–ocean boundary passes through the velocity points and, since the tracer fluxes ($K_v \partial X/\partial z$) are naturally defined on these points, the diffusive flux boundary condition can simply be written

$$K_V \left.\frac{\partial X}{\partial z}\right|_b = \gamma_X (X_b - X_{1/2}), \tag{24}$$

where the subscript 1/2 indicates conditions at the uppermost grid point within the water column, half a grid box below the interface. The lack of tracer points on the boundary is not a problem because the value X_b is derived from (6) and need not be formally assigned to any grid point.

Application of (24) is equivalent to (21) in that, consistent with the assumption of no normal flow at the boundary, it neglects the advection of meltwater across the ice–ocean interface. However, if the tracer budgets are to be closed correctly, the first grid point in from the boundary must feel the additional sinks of heat and salt associated with the advection of meltwater across the boundary layer. Because Eq. (22) is cast in flux form, it would be simple to impose an advective flux at the ice–ocean interface, but the advection field would then be inconsistent with the velocity field, which is derived on the basis of no normal flow at the boundaries. The problem of nonconservation of tracers would be exacerbated. Instead we apply a modified flux boundary condition that is analogous in form to the terms appearing in our earlier layer-integrated equations 15:

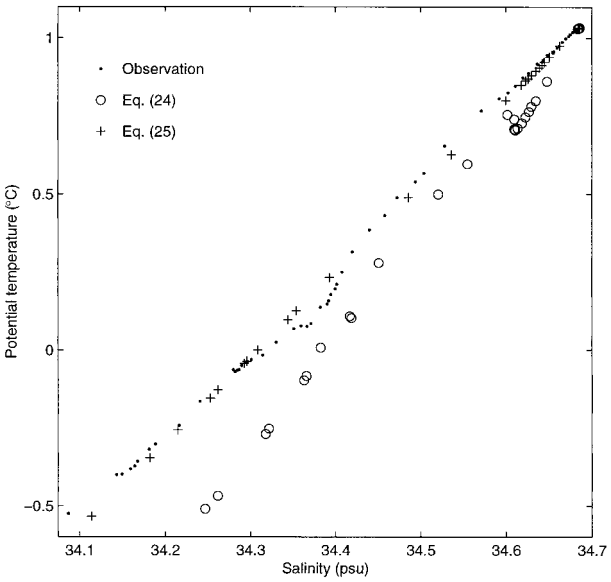

FIG. 8. Potential temperature vs salinity diagram comparing observations made at the calving front of Pine Island Glacier (dots) with the output from a two-dimensional model of thermohaline circulation in the sub-ice cavity (Hellmer et al. 1998). The vertical profiles of potential temperature and salinity used here constitute the open boundary of the model domain. Model results obtained using flux boundary conditions defined as in (24) and (25) are indicated by open circles and crosses, respectively. Both versions of the model were tuned to give net melt rates for the glacier that were consistent with observation.

$$K_V \left.\frac{\partial X}{\partial z}\right|_b = (\gamma_X + m)(X_b - X_{1/2}). \tag{25}$$

Hellmer et al. (1998) applied the two-dimensional model to the water column beneath the 90-km floating extension of Pine Island Glacier, a fast-flowing outlet glacier of the West Antarctic Ice Sheet. Employing flux boundary conditions of the form shown in (25), they were able to obtain good agreement between modeled outflow characteristics and observations made at the calving front of the glacier. Figure 8 shows a comparison between the results of this model run and the observations. The results of a second model run, which employed boundary conditions of the form shown in (24), are also shown in Fig. 8. These latter results are clearly inferior.

The straight line trajectory in potential temperature/salinity space, apparent in Fig. 8, is characteristic of ice melting in seawater. Gade (1979) calculated the gradient of this line to be

$$\frac{\partial T}{\partial S} = \frac{c(T_w - T_b) + L_i + c_i(T_b - T_s)}{c(S_w - S_i)}, \tag{26}$$

where the subscript w indicates the far-field seawater properties and for glacier ice the salinity is zero. The

slope is primarily a function of the water and ice properties and depends only very weakly on the melt rate, through its influence on the boundary temperature. Taking the ratio of heat flux to salt flux, as expressed by (25), substituting from (6), (7), and (23), and setting the salinity of the ice to zero, an expression analogous to (26) is readily obtained. However, writing the fluxes as in (24), a similar procedure leads to

$$\frac{\partial T}{\partial S} = \frac{L_i + c_i(T_b - T_s)}{c(S_b - S_i)}, \tag{27}$$

which represents erroneous forcing on the model. Furthermore, the appearance of the boundary salinity in the denominator makes the slope sensitive to such factors as the melt rate and the magnitude of the turbulent transfer coefficient for salt.

5. Significance for other models

Boundary formulations that include all the effects of meltwater advection are, to our knowledge, uncommon. However, for conditions of low melt/freeze rate and for integrations over short timescales, the errors caused by nonconservation of tracers are probably small. This is the case with most models of the interaction between ice shelves and the ocean, the early versions of which (Hellmer and Olbers 1989; Scheduikat and Olbers 1990; Jenkins 1991) all used boundary formulations analogous to (21) or (24). Later versions of these models (Nicholls and Jenkins 1993; Jenkins and Bombosch 1995; Hellmer et al. 1998) have been corrected, although it is only in the case of the Pine Island Glacier simulations cited in the previous section where melt rates are $\sim$10 m yr^{-1}, an order of magnitude higher than in the other examples, that the correction has had a significant impact on the results.

The literature on coupled sea ice–ocean models is too vast to enable us to present an authoritative survey of all the various boundary formulations in use. In any case, the published descriptions of the models often lack the level of detail required to reveal the use of conservative or nonconservative boundary conditions. Our discussion has centered on what Holland and Jenkins (1999) refer to as three-equation formulations. These employ all of Eqs. (6)–(8) to diagnose the temperature, salinity, and melt/freeze rate at the ice–ocean interface. This type of formulation is not commonly encountered in sea ice models, but where it is, boundary conditions corresponding to (21) and (24) appear to be in use. Two-equation formulations are encountered more often. In these, the salinity at the boundary is assumed equal to that at the upper model level or layer, and only heat transfer through the thermal boundary layer is considered. McPhee et al. (1999) demonstrate that with a suitable choice of effective heat transfer coefficient, such a formulation can yield realistic melt rates. Since the boundary salinity is not explicitly calculated, the conventional choice for the salinity equation is a flux boundary condition of the form

$$K_V \left.\frac{\partial S}{\partial z}\right|_b = m(S_i - S), \tag{28}$$

where S represents the salinity at the uppermost grid point in the water column. This is simply the expression in (25), rewritten using (6), so it is a conservative boundary condition that implicitly includes both advective and diffusive fluxes. However, the analogous boundary condition for temperature, obtained from a combination of (25) and (7),

$$K_V \left.\frac{\partial T}{\partial z}\right|_b = m\left(T_b - T - \frac{L}{c}\right) + \left.\frac{K_i}{\rho c}\frac{\partial T_i}{\partial z}\right|_b, \tag{29}$$

is rarely seen. The conventional version of (29) includes only the latent heat term and the heat conduction through the ice, and therefore conforms to the nonconservative form of (24). Incorporation of meltwater advection into the salt balance eliminates the dominant source of error, but the advection term can rise to several percent of the latent heat term in (29). Although uncertainties in the latent heat term itself may still dominate the overall error in the heat flux, errors resulting from such uncertainty are of opposite sign for melting and freezing, whereas the error arising from neglect of the advective term is independent of the sign of the phase change.

More generally, ice–ocean models often include additional processes such as percolation of surface meltwater through to the ice–ocean interface and precipitation and evaporation at the surface of leads. If percolating meltwater is assumed to have the salinity of the ice and be at the freezing point, Eqs. (6) and (7) become

$$\rho\gamma_S(S - S_b) = \rho(m + m_p)(S_b - S_i) \tag{30}$$

$$\rho_i c_i k_i \left.\frac{\partial T_i}{\partial z}\right|_b + \rho c\gamma_T(T - T_b) = \rho m L_i + \rho c m_p(T_b - T_{fi}), \tag{31}$$

where m_p is the percolation velocity, which is either specified or derived from an ice model, and T_{fi} is the freezing point appropriate for a salinity of S_i. The vertical velocity at the ice–ocean interface, taken as the level of the mean ice draft, is expressed as

$$w_b = \frac{\partial z_b}{\partial t} + \mathbf{u}_b \cdot \nabla z_b - A(m + m_p) - (1 - A)(p - e), \tag{32}$$

where p and e represent the rates of precipitation and evaporation respectively. We could now either apply separate advective and diffusive boundary conditions based on these, as in section 3, or, if we wished to maintain the simplicity of a material ice–ocean interface, we could apply a combined flux boundary con-

dition of the form given in (25). For salinity this would read

$$K_V \frac{\partial S}{\partial z}\bigg|_b = A(\gamma_S + m + m_p)(S_b - S) - (1 - A)(p - e)S. \quad (33)$$

Again we emphasize, by substitution from (30), that this yields the conservative boundary condition:

$$K_V \frac{\partial S}{\partial z}\bigg|_b = A(m + m_p)(S_i - S) - (1 - A)(p - e)S. \quad (34)$$

In contrast, neglect of the meltwater advection terms in (33) yields a boundary condition analogous to (24),

$$K_V \frac{\partial S}{\partial z}\bigg|_b = A\gamma_S(S_b - S) - (1 - A)(p - e)S, \quad (35)$$

and leads, on substitution from (30), to the nonconservative form:

$$K_V \frac{\partial S}{\partial z}\bigg|_b = A(m + m_p)(S_i - S_b) - (1 - A)(p - e)S. \quad (36)$$

In a two-equation formulation (34) would be the natural choice, but we note that the advection of percolating meltwater into the ocean has an impact on the ice–ocean heat flux, equivalent to the addition of the term $m_p(T_{fi} - T)$ to the right-hand side of (29), that is likely to be overlooked. This term would generally be small but, since the interfacial melt rate and percolation velocity are unrelated, it is possible that under certain conditions it could be the dominant term in the ice–ocean heat flux.

Larger-scale ice–ocean models often use a simpler one-equation formulation in which only the freezing point at the upper level or layer of the model is diagnosed. At each time step the computed temperature is reset to the freezing point and an appropriate amount of ice melted or frozen. Once again, because a separate boundary salinity is not calculated, the salinity balance is almost certainly computed correctly, but we suspect that the much smaller errors in the heat balance are routinely made. Of course, none of the errors discussed in this paper will be apparent in models that employ either surface restoring fluxes or diagnosed flux corrections, which are specifically designed to eliminate drift such as that in Figs. 5 and 7.

6. Closing remarks

Mellor et al. (1986) concluded that for small $|m/u_*|$, where u_* is the surface friction velocity, it is possible to neglect the influence of vertical advection in the formulation of boundary conditions at an ice–ocean interface. However, this conclusion was based on an assessment of the likely impact of vertical advection on the structure of the boundary layer. We do not dispute this finding and have implicitly made use of it in our parameterization of diffusion through the boundary layer. Nevertheless, we conclude that meltwater advection does play a role in the balance equations for tracers within a sub-ice water column and that this role may be neglected only if $|m/\gamma_X|$ is small. Since $\gamma_S/u_* \approx 4 \times 10^{-4}$ and the turbulent transfer coefficients for most other dissolved species are of a similar order of magnitude to that of salt, this latter criterion is a much more stringent requirement. We conclude that in general it is not possible to neglect the impact of meltwater advection.

We have presented a formulation of the flux boundary condition at an ice–ocean interface that includes both advective and diffusive fluxes and have demonstrated that inclusion of the advective term is necessary for the conservation of tracers. In practice, the advective fluxes are likely to be excluded only if the application of the boundary conditions involves the explicit diagnosis of the tracer concentration at the ice–ocean interface. There are relatively few models that include this level of sophistication and, although the heat flux error is an exception in that its occurrence is likely in almost all formulations, it is also the least significant of the errors. For other tracers, the commonly used boundary conditions already incorporate both advective and diffusive fluxes, but we believe the foregoing discussion to be of more than academic interest. As computing resources become ever more readily available, more detailed representations of key physical processes are likely to become part of even global-scale models. While our current knowledge of ice–ocean boundary physics is not sufficient to say with confidence that melting and freezing can be calculated more accurately if the boundary salinity is explicitly diagnosed, the inclusion of some additional tracers, in particular stable isotopes, does require the computation of the their boundary concentrations. Also, if the use of a nonmaterial interface at the ocean surface, as recommended by Huang (1993), becomes more commonplace, the distinction between the advective and diffusive parts of the tracer fluxes will become important. If a separate advective boundary condition is applied to the scalar equations, the purely diffusive flux boundary condition (24) must be employed to avoid double-counting of the meltwater advection term. Finally, as efforts are already being made to eliminate the need for flux corrections in coupled ocean–atmosphere general circulation models, it is important to isolate all possible causes of spurious drift in the properties of the ocean.

Acknowledgments. This study would not have been undertaken were it not for the attentive reading and constructive criticism of some of the authors' earlier work by others. Andreas Bombosch and Gregory Lane-Serff independently pointed out the inconsistency in Jenkins (1991). Chris Garrett, in his role as associate editor for an earlier version of Hellmer et al. (1998), asked a number of perceptive questions about the model

behavior. In addressing these we became aware of the possible size of the errors we have described. We gratefully acknowledge this invaluable input. Miles McPhee kindly supplied us with the data from the Snowbird ice station, used to generate Fig. 3, and provided an insightful review of the manuscript. We would like to thank Aike Beckmann, Ralph Timmermann, Keith Nicholls, Chris Doake, and Rupert Gladstone for reading through earlier versions of this paper. Their comments lead to significant clarification of a number of points. Collaborative work that gave rise to this paper was supported by U.S. Department of Energy Grant DE-FG02-93-ER61716 and NASA Polar Programs research Grant NAG5-4028.

APPENDIX

How Large Are the Errors?

The error in the tracer flux, per unit area of ice cover, associated with the use of boundary conditions of the form given in (21) and (24) is

$$Q_{X\mathrm{err}} = -\rho m(X_b - X), \tag{A1}$$

which, using (6) and ignoring the diffusive flux into the ice, can be rewritten:

$$Q_{X\mathrm{err}} = \rho\frac{m^2}{\gamma_X}(X_b - X_i). \tag{A2}$$

For tracers that are rejected from the ice on freezing, the drift will be toward higher concentrations. For equivalent melt/freeze rates the drift will tend to be slightly faster during freezing, when the boundary concentration is raised, than during melting, when the boundary is depleted in the tracer. By substituting for the melt rate from (7) we can express the error as

$$Q_{X\mathrm{err}} = \frac{(X_b - X_i)}{\rho\gamma_X L_i^2}\left[\rho c\gamma_T(T - T_b) + \rho_i c_i k_i\frac{\partial T_i}{\partial z}\bigg|_b\right]^2. \tag{A3}$$

The error in the heat flux is expressed

$$Q_{h\mathrm{err}} = -\rho cm(T_b - T), \tag{A4}$$

and, substituting directly for the melt rate, we obtain

$$Q_{h\mathrm{err}} = \frac{c(T - T_b)}{L_i}\left[\rho c\gamma_T(T - T_b) + \rho_i c_i k_i\frac{\partial T_i}{\partial z}\bigg|_b\right]. \tag{A5}$$

The external factors that determine the melt/freeze rate are the level of turbulence in the mixed layer, how far the temperature of the mixed layer deviates from the freezing point, and the temperature gradient in the ice. We focus on the salt and heat flux errors and seek to express (A3) for salinity and (A5) in terms of the above three factors. The level of turbulence determines the magnitude of the transfer coefficients for heat and salt, an effect that we parameterize by making γ_T a linear function of the friction velocity, u_*,

$$\gamma_T = C_h u_*, \tag{A6}$$

and setting the ratio γ_S/γ_T to a constant value. We take values of 0.01 for the factor C_h and 0.04 for the ratio γ_S/γ_T (McPhee et al. 1999; Holland and Jenkins 1999).

We consider first a situation, such as that addressed in the model described in section 3, in which the heat conduction term is negligible and to a good approximation we can assume melting and freezing to be driven entirely by temperature variations in the water column. Under these conditions, we can ignore the first terms on the left-hand side of both (6) and (7) and hence obtain a simple expression for the ratio of the salinity to temperature difference across the boundary layer:

$$\frac{(S_b - S)}{(T_b - T)} = \frac{(S_b - S_i)c\gamma_T}{L_i\gamma_S}. \tag{A7}$$

We refer to the elevation of the far-field temperature above the freezing point as the thermal driving,

$$T_* = T - \lambda_1 S - \lambda_2 - \lambda_3 P_b, \tag{A8}$$

and, using (8), we relate this to the temperature difference across the boundary layer:

$$T_b - T = \lambda_1(S_b - S) - T_*. \tag{A9}$$

Using (A7) we can rewrite this as

$$T - T_b = \frac{T_*}{\Lambda}, \tag{A10}$$

where

$$\Lambda = 1 - \frac{\lambda_1(S_b - S_i)c\gamma_T}{L_i\gamma_S}. \tag{A11}$$

This rearrangement is the origin of the effective heat transfer coefficient, defined in (17). With (A6) and (A10) substituted into (A3) and (A5) we obtain

$$Q_{X\mathrm{err}} = \frac{C_h(X_b - X_i)}{\rho(\gamma_X/\gamma_T)}u_*\left(\frac{\rho c}{L_i\Lambda}T_*\right)^2, \quad \text{and} \tag{A12}$$

$$Q_{h\mathrm{err}} = \frac{C_h}{\rho L_i}u_*\left(\frac{\rho c}{\Lambda}T_*\right)^2, \tag{A13}$$

where the temperature gradient terms within the parentheses of (A3) and (A5) have been set to zero, consistent with our assumption of negligible heat conduction.

Holland and Jenkins (1999) demonstrate that for thermal driving of <0.5°C, the small variations in boundary salinity have little impact on the effective heat transfer [Eq. (17)]. Taking S_b in (A11) to be constant at 34.5 psu, and taking the ice salinity to be zero, Λ has a constant value of 1.59. The only remaining variables in (A12) and (A13) are then the thermal driving, the friction velocity, and the difference in tracer concentration between the ice and the boundary. To evaluate the salt flux error we make the same approximations for the boundary and ice salinities. We then replace all constants in (A12) and (A13) with their numerical values

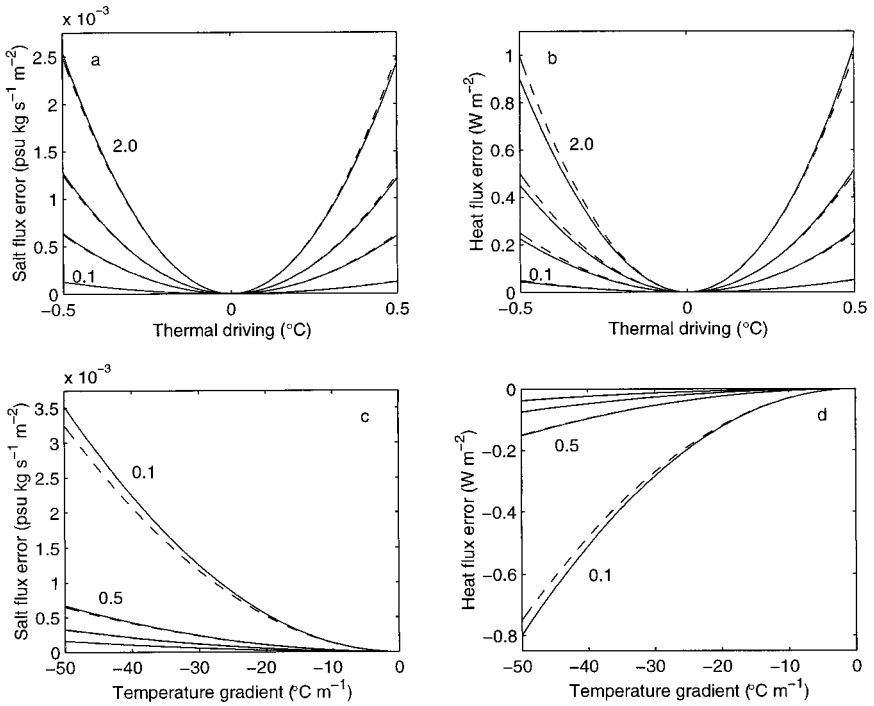

FIG. A1. Salt and heat flux errors induced by the neglect of meltwater advection across an ice–ocean boundary for friction velocities of 0.1, 0.5, 1.0, and 2.0 cm s^{-1}: (a) salt flux errors defined by (A12) (solid line) and by the approximation (dashed line) given in (A14a), (b) heat flux errors defined by (A13) (solid line) and by the approximation (dashed line) given in (A14b), (c) salt flux errors defined by (A17) (solid line) and by the approximation (dashed line) given in (A19a), and (d) heat flux errors defined by (A18) (solid line) and by the approximation (dashed line) given in (A19b).

and express the salt and heat flux errors, respectively, as

$$Q_{S\mathrm{err}} \approx 0.5 u_* T_*^2 \quad [\mathrm{psu\ kg\ s^{-1}\ m^{-2}}] \qquad \text{(A14a)}$$

$$Q_{h\mathrm{err}} \approx 200 u_* T_*^2 \quad [\mathrm{W\ m^{-2}}], \qquad \text{(A14b)}$$

where u_* is in meters per second and T_* is in degrees Celsius.

We next consider the alternative situation where the thermal driving is zero and freezing proceeds as a result of the heat conducted into the cold ice above. Under these conditions we can combine (6) for salinity with (A9) to give an expression for the melt rate,

$$m = \frac{\gamma_S}{\lambda_1 (S_b - S_i)} (T - T_b), \qquad \text{(A15)}$$

and substituting this into (7) we can express the temperature difference across the oceanic boundary layer in terms of the temperature gradient at the base of the ice:

$$T - T_b = \frac{(1 - \Lambda)}{\Lambda} \frac{\rho_i c_i k_i}{\rho c \gamma_T} \left. \frac{\partial T_i}{\partial z} \right|_b . \qquad \text{(A16)}$$

With (A6) and (A16) substituted into (A3) and (A5) we obtain

$$Q_{X\mathrm{err}} = \frac{(X_b - X_i)}{\rho C_h (\gamma_X / \gamma_T)} \frac{1}{u_*} \left(\frac{\rho_i c_i k_i}{L_i \Lambda} \left. \frac{\partial T_i}{\partial z} \right|_b \right)^2 \quad \text{and} \qquad \text{(A17)}$$

$$Q_{h\mathrm{err}} = \frac{(1 - \Lambda)}{\rho C_h L_i} \frac{1}{u_*} \left(\frac{\rho_i c_i k_i}{\Lambda} \left. \frac{\partial T_i}{\partial z} \right|_b \right)^2 . \qquad \text{(A18)}$$

Making the same approximations as before, the salt and heat flux errors can be written, respectively

$$Q_{S\mathrm{err}} \approx \frac{1.3 \times 10^{-9}}{u_*} \left(\left. \frac{\partial T_i}{\partial z} \right|_b \right)^2 \quad [\mathrm{psu\ kg\ s^{-1}\ m^{-2}}] \qquad \text{(A19a)}$$

$$Q_{h\mathrm{err}} \approx \frac{-3 \times 10^{-7}}{u_*} \left(\left. \frac{\partial T_i}{\partial z} \right|_b \right)^2 \quad [\mathrm{W\ m^{-2}}], \qquad \text{(A19b)}$$

where, once again, u_* is in meters per second and the temperature gradient is in degrees Celsius.

The salt and heat flux errors given by (A12), (A13), (A14), (A17), (A18), and (A19) are plotted in Fig. A1 for a range of values of friction velocity, thermal driving, and basal temperature gradient. The quadratic dependence on the latter two factors means that the errors are always of the same sign. In the case of (A14) the effects of the errors are counteractive, in that the heat flux error should cause melting and dilution of the mixed

layer, while the salt flux error acts to increase the mixed layer salinity. In the case of (A19), both errors serve to accentuate the effects of freezing. We note that however the errors combine and whichever is dominant, the effect is most evident in the computed salinity because the properties of the seawater are constrained to follow closely the liquidus, which has an almost flat trajectory in temperature/salinity space.

REFERENCES

Gade, H. G., 1979: Melting of ice in sea water: A primitive model with application to the Antarctic ice shelf and icebergs. *J. Phys. Oceanogr.*, **9,** 189–198.

Hellmer, H. H., and D. J. Olbers, 1989: A two-dimensional model for the thermohaline circulation under an ice shelf. *Antarct. Sci.*, **1,** 325–336.

——, S. S. Jacobs, and A. Jenkins, 1998: Oceanic erosion of a floating Antarctic glacier in the Amundsen Sea. *Ocean, Ice, and Atmosphere: Interactions at the Antarctic Continental Margin*, S. S. Jacobs and R. F. Weiss, Eds., Antarctic Research Series, Vol. 75, Amer. Geophys. Union, 83–99.

Holland, D. M., and A. Jenkins, 1999: Modeling thermodynamic ice–ocean interactions at the base of an ice shelf. *J. Phys. Oceanogr.*, **29,** 1787–1800.

Huang, R. X., 1993: Real freshwater flux as a natural boundary condition for the salinity balance and thermohaline circulation forced by evaporation and precipitation. *J. Phys. Oceanogr.*, **23,** 2428–2446.

Jenkins, A., 1991: A one-dimensional model of ice shelf–ocean interaction. *J. Geophys. Res.*, **96,** 20 671–20 677.

——, and A. Bombosch, 1995: Modeling the effects of frazil ice crystals on the dynamics and thermodynamics of Ice Shelf Water plumes. *J. Geophys. Res.*, **100,** 6967–6981.

Josberger, E. G., 1983: Sea ice melting in the marginal ice zone. *J. Geophys. Res.*, **88,** 2841–2844.

Maykut, G. A., and M. G. McPhee, 1995: Solar heating of the Arctic mixed layer. *J. Geophys. Res.*, **100,** 24 691–24 703.

McPhee, M. G., 1983: Turbulent heat and momentum transfer in the oceanic boundary layer under melting pack ice. *J. Geophys. Res.*, **88,** 2827–2835.

——, 1990: Small-scale processes. *Polar Oceanography, Part A: Physical Science*, W. O. Smith Jr., Ed., Academic Press, 287–334.

——, G. A. Maykut, and J. H. Morison, 1987: Dynamics and thermodynamics of the ice/upper ocean system in the marginal ice zone of the Greenland Sea. *J. Geophys. Res.*, **92,** 7017–7031.

——, C. Kottmeier, and J. H. Morison, 1999: Ocean heat flux in the central Weddell Sea during winter. *J. Phys. Oceanogr.*, **29,** 1166–1179.

Mellor, G. L., M. G. McPhee, and M. Steele, 1986: Ice–seawater turbulent boundary layer interaction with melting and freezing. *J. Phys. Oceanogr.*, **16,** 1829–1846.

Millero, F. J., 1978: Annex 6: Freezing point of seawater. Eighth Report of the Joint Panel of Oceanographic Tables and Standards, UNESCO Tech. Paper Mar. Sci. 28, 29–31.

Nicholls, K. W., and A. Jenkins, 1993: Temperature and salinity beneath Ronne Ice Shelf, Antarctica. *J. Geophys. Res.*, **98,** 22 553–22 568.

Nøst, O. A., and A. Foldvik, 1994: A model of ice shelf–ocean interaction with application to the Filchner-Ronne and Ross Ice Shelves. *J. Geophys. Res.*, **99,** 14 243–14 254.

Scheduikat, M., and D. J. Olbers, 1990: A one-dimensional mixed layer model beneath the Ross Ice Shelf with tidally induced vertical mixing. *Antarct. Sci.*, **2,** 29–42.

Steele, M., G. L. Mellor, and M. G. McPhee, 1989: Role of the molecular sublayer in the melting or freezing of sea ice. *J. Phys. Oceanogr.*, **19,** 139–147.